# Transition from *n*- to *p*-Type of Spray Pyrolysis Deposited Cu Doped ZnO Thin Films for NO$_2$ Sensing

M. B. Rahmani[1, 2, *], S. H. Keshmiri[2], M. Shafiei[1], K. Latham[3], W. Wlodarski[1], J. du Plessis[4], and K. Kalantar-Zadeh[1]

[1]*Sensor Technology Laboratory, RMIT University, Melbourne, Australia*
[2]*Microelectronics Research Laboratory, Physics Department, School of Sciences, Ferdowsi University of Mashhad, Mashhad, Iran*
[3]*Applied Chemistry, School of Applied Sciences, RMIT University, Melbourne, Australia*
[4]*Applied Physics, School of Applied Sciences, RMIT University, Melbourne, Australia*

The structural, optical, and gas-sensing properties of spray pyrolysis deposited Cu doped ZnO thin films were investigated. Gas response of the undoped and doped films to NO$_2$ (oxidizing) gas shows an increase and decrease in resistance, respectively, indicating *p*-type conduction in doped samples. The UV-Vis spectra of the films show decrease in the bandgap with increasing Cu concentration in ZnO. The observed *p*-type conductivity is attributed to the holes generated by incorporated Cu atoms on Zn sites in ZnO thin films. The X-ray diffraction spectra showed that samples are polycrystalline with the hexagonal wurtzite structure and increasing the concentration of Cu caused a decrease in the intensity of the dominant (002) peak. The surface morphology of films was studied by scanning electron microscopy and the presence of Cu was also confirmed by X-ray photoelectron spectroscopy. Seebeck effect measurements were utilized to confirm the *p*-type conduction of Cu doped ZnO thin films.

**Keywords:** Gas Sensors, Zinc Oxide, Cu Doping, Spray Pyrolysis.

**RESEARCH ARTICLE**

## 1. INTRODUCTION

Wurtzite ZnO is a wide-bandgap metal oxide semiconductor with a direct energy gap of approximately 3.3 eV. This bandgap can be tuned in a range between 3.0 to 4.0 eV by doping with metals such as Cd and Mg.[1–3] ZnO is one of the most important II–VI compound semiconductors with many applications in the fabrication of devices including ultraviolet (UV) light-emitters, varistors, transparent high-power electronics, piezoelectric transducers, gas-sensors, smart windows and solar cells.[4] As-grown ZnO usually exhibits *n*-type conductivity, and the cause of this residual doping is heavily debated. Some of the possible origins for the native *n*-background doping of ZnO include the incorporation of impurities (e.g., F, Cl on the O site, B, Al, Ga on the Zn site, or hydrogen), existence of native point defects (e.g., antisite, interstitial, vacancy) and structural defects.[5] However, in order to fully use ZnO potential for

the fabrication of optoelectronic devices, access to *p*-type ZnO of highly controlled properties is desirable.

A potential *p*-type doping candidate for ZnO is Cu. Cu, as a group Ib element (Cu, Ag and Au), can assume a valency of either +1 or +2 depending on its chemical configuration, for example in the compounds Cu$_2$O and CuO, respectively. The radii of Cu$^+$ (98 pm) and Cu$^{2+}$ (80 pm) ions are similar to that of Zn$^{2+}$ ion (83 pm), compared with that of Ag$^+$ ion (113 pm) in the same Ib group.[6] If Cu is needed to become an acceptor upon the substitution at a Zn site, it will have to assume a valency of +1.[7] It is known that group Ib metals are fast-diffusing in compound semiconductors. The diffusion of Cu into ZnO can cause the formation of complex centres (Cu$_{Zn}$, Cu$_i$). It is possible that Cu atoms can replace either substitutional or interstitial Zn atoms in the ZnO lattice creating structural deformations.[8, 9] Cu significantly affects the electrical, chemical, structural and optical properties of ZnO, and the study of the electronic state of Cu in ZnO has been the subject of interest for a long time.[6, 10–12]

---

*Corresponding author; E-mail: mb.rahmani@stu-mail.um.ac.ir

Metal oxide semiconductors (such as SnO$_2$,[13] ZnO,[14, 15] In$_2$O$_3$,[16] WO$_3$,[17, 18] TiO$_2$,[19] Sb$_x$O$_y$[20] and MoO$_3$[21]) have attracted significant attention towards gas sensing due to their simple implementation, low cost, and good reliability for real-time control systems with respect to other gas sensors. The gas sensing properties of metal oxide semiconductors are influenced by many factors such as their operating temperatures, morphology and chemical composition of the films.[22] In such gas sensors the change in the electrical conductivity is due to the interaction of the targeted gas molecules (chemi or physisorption) with the surface of the metal oxide grains. Consequently, metal oxide sensors show changes in the resistance under exposure to oxidizing or reducing gases.[17, 23, 24] Since the majority of these sensitive layers are *n*-type, *p*-type semiconductors sensitive to gases are highly demanded for gas sensing applications such as sensor arrays for electronic nose. These *p*-type semiconductor gas sensors have much different sensing pattern from their *n*-type counterparts.[25] In addition, it is also reported that *p*-type semiconductors are more appropriated for detecting oxidizing gases such as NO$_2$.[26] NO$_2$ is a highly reactive gas showing oxidizing characteristics. At elevated temperatures, the presence of chemically adsorbed molecules such as NO$_2$ can cause electron depletion at the surface of the metal oxide grains; and consequently, the electrical resistivity of the thin films increases.[15] The competition between chemisorptions of NO$_2$ and atmospheric oxygen O$_2$, at the same active surface sites of the metal oxide layer, plays an important role in determining the specific NO$_2$/metal oxide interaction.[27]

In this work, spray pyrolysis technique has been used for the deposition of ZnO thin films with different Cu doping concentrations for NO$_2$ sensing. Several techniques such as sputtering,[28, 29] pulsed laser deposition,[30] sol–gel technique,[31] and spray pyrolysis[8, 32] have been applied for the deposition of undoped and doped ZnO films. In comparison, spray pyrolysis can be cheaper, simpler and more versatile than the others techniques. The properties of the sprayed films can be easily tuned for required applications. Additionally, it is also a suitable deposition method when large areas films are needed. Seebeck effect measurements were employed to confirm the *p*-type conduction of Cu doped ZnO thin films. Thin films were characterized using X-ray diffraction (XRD), scanning electron microscopy (SEM), X-ray photoelectron spectroscopy (XPS) and UV-Vis spectrometry techniques. The effects of different concentrations of Cu on the electrical, structural, optical, and NO$_2$ gas sensing properties of the ZnO films have been investigated.

## 2. EXPERIMENTAL DETAILS

### 2.1. Thin Film Deposition

The Cu doped ZnO thin films were deposited on glass substrates at a fixed substrate temperature of 450 °C using a typical spray pyrolysis coating system.[33, 34] The precursor solution (100 ml) was prepared by dissolving 0.15 M of zinc acetate dihydrate [Zn(CH$_3$COO)$_2 \cdot$ 2H$_2$O] and different concentrations of copper chloride dihydrate (CuCl$_2 \cdot$ 2H$_2$O) in solvent of mixture of double DI water and isopropyl alcohol in a volume ratio of 1:3. To enhance the solubility of zinc acetate, 0.4 ml of acetic acid was also added to the solution. The atomic ratio of [Cu]/[Zn] in a range of 0 to 20 at% was prepared (0, 0.5, 1, 2, 4, 8, 16 and 20 at%).

Before the deposition of the films, glass substrates were cleaned and placed on the hot plate (450 °C). The undoped and Cu doped films were deposited on rotating (25 rpm) hot substrates using the pyrolysis technique. The solutions were sprayed using a 0.2 mm nozzle with the help of N$_2$ carrier gas. The solutions flow rate, carrier gas pressure and nozzle to substrate distance were held constant at 10 ml/min, 2 atm and 40 cm, respectively. All experiments were performed under similar conditions. Film thicknesses were determined to be approximately 300 nm using a profilometer (Ambios-Technology XP-2).

For the conductometric sensors fabrication, the sensing area was covered with a physical mask and then a layer of gold with the thickness of 100 nm was sputtered to make contact pads. Afterwards, two gold wires were bonded to the gold pads using silver epoxy.

### 2.2. Electrical and Seebeck Effect Measurements

The gas sensing measurements were conducted at elevated temperatures. As a result, in order to determine the type of the majority of carriers at these temperatures, the Seebeck effect measurements were performed.[35] All samples were heated to a constant temperature of 135 °C using a hot plate and then a temperature difference between their two electrodes was produced using a spot heater. The temperatures between hot and cold electrodes ($\Delta T$) were continuously measured using $K$ type thermocouples. The voltage difference ($\Delta V$) across the electrodes was measured using a multimeter (Keithley 2001). Consequently, the Seebeck coefficient, $S$, was calculated using $S = \Delta V / \Delta T$.

### 2.3. Structural and Morphological Characterizations

X-ray powder diffraction (Bruker D8 ADVANCE) was used for structural analysis for Bragg angles ($2\theta$) ranging from 5° to 90° using Cu K$\alpha$ radiation ($\lambda = 1.5406$ Å). The elemental composition and chemical state of copper in Cu doped ZnO films was investigated by X-ray photoelectron spectroscopy (XPS) on a VG-310F photoelectron spectrometer using the Al K$\alpha$ excitation line of 1486 eV. Spectra were obtained after etching with 3 keV Ar$^+$ ions which also resulted in additional charging. After prolonged sputtering, the adventitious carbon was also removed and another constant peak had to be chosen as a reference for charge correction. For this study, the Zn 2p$_{3/2}$ peak at

1022.1 eV ZnO was chosen and all spectra were corrected using this value.[36] Spectra were taken at room temperature. The surface morphology of films was studied using SEM images (FEI Nova NanoSEM-200).

## 2.4. Optical Properties

The optical transmission spectra of the samples were obtained in the ultraviolet (UV)/visible (VIS)/near infrared (NIR) regions up to 1100 nm using a UV-VIS spectrometer (Ocean Optics HR4000CG-UV-NIR). The measurements were carried out in the wavelength scanning mode at room temperature and using uncoated glass as the reference.

## 2.5. Gas Sensing Measurements

Undoped ZnO and Cu doped ZnO conductometric sensors were mounted on a heater, separately. The heater was controlled by a regulated DC power supply providing different operating temperatures. The output resistance as a function of time across the conductometric sensor during NO₂ exposure was measured using a multimeter (Keithley 2001). A computerized gas calibration system, with mass flow controllers, was used for exposing the sensor to different concentrations of NO₂ gas. The total flow rate was kept constant at 200 sccm and dry synthetic air was used as the reference gas. At each operating temperature, the baseline gas was maintained for a duration of 120 min to allow the device to stabilize. Then, the device was exposed to sequences of different concentrations of NO₂ for several hours. The sensor temperature was varied in the 20–260 °C range. Each NO₂ gas sequence consisted of 0.6, 1.25, 2.5, 5 and 10 ppm balanced in synthetic air. A second pulse of 1.25 ppm was utilized to confirm its repeatability. If $R_g$ and $R_0$ denote the resistance of the sensor in the presence of gas and in air, respectively, then the response factor was defined as $(R_g - R_0)/R_0$.

## 3. RESULTS AND DISCUSSION

### 3.1. Seebeck Coefficient and Sheet Resistance

Table I presents the measured Seebeck coefficients for undoped and Cu doped ZnO thin films. The Seebeck coefficient value is negative for undoped ZnO and is positive for Cu doped ZnO samples, indicating *n*-type and *p*-type conductions, respectively. For higher concentrations of Cu in ZnO, we see larger values for Seebeck coefficients, this

**Table I.** Seebeck coefficients (*S*) of undoped and Cu doped ZnO films.

| Sample | $S$ ($\mu$V/K) | Conduction type |
|---|---|---|
| ZnO | −125 | *n* |
| ZnO: 1 at% Cu | +31 | *p* |
| ZnO: 8 at% Cu | +192 | *p* |
| ZnO: 20 at% Cu | +325 | *p* |

increase can be due to the formation of other phases such as CuO or Cu₂O which are *p*-type semiconductors.[37]

A high dc electrical resistance in the order of GΩ was observed for films at temperatures below 100 °C. This can be attributed to the large density of extrinsic traps at the ZnO grain boundaries due to the presence of oxygen.[38] These traps deplete the surface of grains and result in a charge carrier barrier at the grain boundaries. The variation in the sheet resistance (in Ω/□) of the films with temperature is shown in Figure 1. For all films, the sheet resistance was found to decrease with increasing temperature. The decrease in resistance is related to the increase in carrier concentration resulting from the activation of deep and shallow carriers which may arise due to native defects such as interstitial Zn/Cu atoms and oxygen vacancies.[38] The ionization of deep neutral defects ($Cu_{Zn}$ and $Zn_i$) requires high energy ($\sim$3.0 eV) and the presence of this type of complex defects might be a reason for the high resistance of doped samples at lower temperatures.[39]

### 3.2. Structural Analysis

Figure 2 shows the XRD patterns of the Cu doped ZnO films deposited at 450 °C. The five diffraction peaks of the ZnO films appear at 31.77, 34.43, 36.27, 47.53, and 62.83° 2$\theta$, which correspond to the (100), (002), (101), (102) and (103) planes, respectively. The intense peaks in the XRD pattern of samples clearly show the formation of the hexagonal wurtzite phase of ZnO having prominent (002) plane in all samples, which is the most stable phase of ZnO.[8]

It was also observed that with increasing the concentration of Cu (from 0 to 20 at%) the intensity of the ZnO peaks decreased and hence the crystallinity of ZnO decreased. The (002) peak positions of the six samples (Table II) were 34.43, 34.46, 34.47, 34.51, 34.52, and 34.70° 2$\theta$, respectively. The shift in the (002) peak for higher Cu concentrations might be due to the substitution of Zn by Cu in the hexagonal lattice. Correspondingly, using the lattice constant *d* of the samples, which could
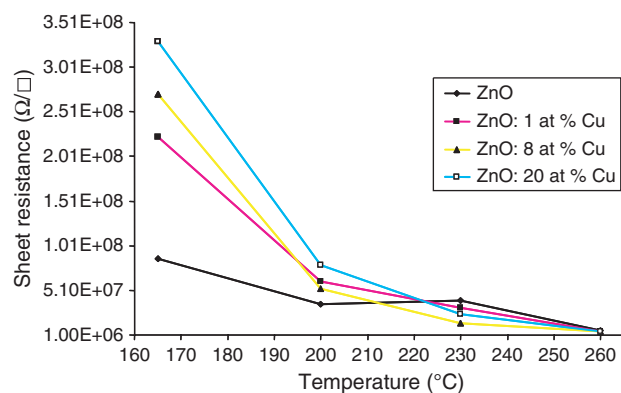


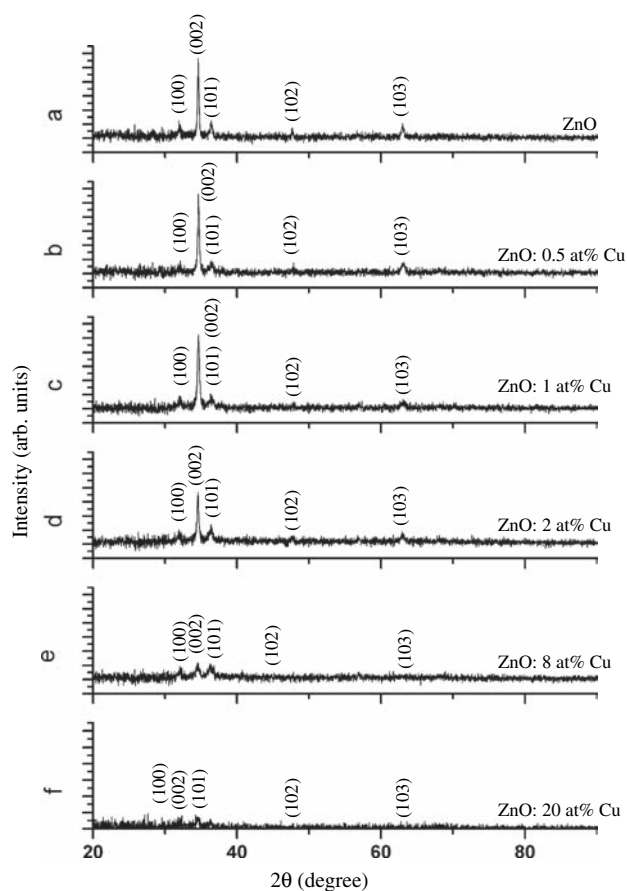**Fig. 1.** Sheet resistance as a function of temperature at different concentrations of Cu.

**Fig. 2.** XRD patterns of Cu doped ZnO thin films with different doping concentrations.

**Table II.** XRD parameters and mean crystallite size for (002) plane at different Cu concentrations.

| Sample | $2\theta$ | Max intensity | $c$ (Å) | FWHM | $D$: crystallite size (nm) |
|---|---|---|---|---|---|
| ZnO | 34.43 | 564 | 5.208 | 0.22 | 38 |
| ZnO: 0.5 at% Cu | 34.46 | 563 | 5.203 | 0.28 | 30 |
| ZnO: 1 at% Cu | 34.47 | 521 | 5.201 | 0.32 | 26 |
| ZnO: 2 at% Cu | 34.51 | 368 | 5.195 | 0.28 | 30 |
| ZnO: 8 at% Cu | 34.52 | 120 | 5.194 | 0.54 | 15 |
| ZnO: 20 at% Cu | 34.70 | 72 | 5.168 | 0.52 | 16 |

be calculated by Bragg formula, lattice parameter (*c*) has been calculated for hexagonal phase[40] which are 5.208, 5.203, 5.201, 5.195, 5.194 and 5.168 Å, respectively.

The mean diameter *D* of the thin films crystallite size was determined by the Scherrer's formula:[12]

$$D = 0.9\lambda/\beta\cos\theta \qquad (1)$$

where $\lambda = 1.5406$ Å which is the wavelength of the X-ray radiation used and $\beta$ is the angular full width of the diffraction peak at the half maximum (FWHM) for the diffraction angle $2\theta$ (Table II). With the increasing of the amount of Cu, crystallite size decreased, FWHM of the (002) peak became wider and the orientation poorer. Increasing of FWHM with Cu doping concentration suggests degradation in crystal quality.[41, 42] As can be seen in the SEM images of Figure 3, the incorporation of Cu correlates with a change in the surface morphology and crystallite size.

### 3.3. XPS and SEM Investigations

Table III shows the XPS elemental analysis the amount of Cu in ZnO: Cu thin films. Measurements on the surface of samples show lower amount of Cu in the films, comparing to the expected or doped amount. The binding energy of Cu 2p$_{3/2}$ was 933.5 (FWHM $\cong$ 1.9 eV), 933.1, 933.3, 933.1, 933.0, 932.8 eV for 1, 2, 4, 8, 16 and 20 at% of Cu in ZnO Cu samples, respectively. The Cu peak at 933.5 eV for 1 at% dopant level corresponds to CuO.[36] For higher dopant levels the peak broadens and shifts to lower binding energies which would be indicative of Cu$_2$O. However, no separate peak component for Cu$_2$O is detected at 932.5 eV—just the gradual broadening of the Cu 2p$_{3/2}$ peak.[12, 36, 37]

The SEM micrographs in Figures 3(a–f) show the morphologies of undoped and Cu doped ZnO films (0.5, 1, 2, 8 and 20 at%). As can be seen, the undoped ZnO film is made of polygonal grains with dimensions in the range of 40–400 nm. After the addition of the Cu at low doping concentrations (0.5 and 1 at%) a secondary morphology phase with different dimensions was observed. However, further addition of Cu dopant (2 and 8 at%) produces a third type morphology of grains which are smaller in dimensions. Interestingly at 20 at% Cu, a combination of large and small grains is observed.

### 3.4. Optical Measurements

The transmittance spectra of the thin films were obtained in the range of 300–900 nm. The average values for the transmittance of ZnO, ZnO: 8 at% Cu and ZnO: 20 at% Cu samples in visible range (400–700 nm) were ~89%, ~87% and ~77%, respectively. As can be seen with increasing the dopant concentration, the transmittance of the films is decreased. The films with lower Cu concentration have higher transmittances and sharper absorption edges.

Yan et al.[10] have reported that the Cu 3*d* orbital is much shallower than the Zn 3*d* orbital. When a Cu atom occupies a Zn site in ZnO, it introduces two main effects: (1) the strong *d*–*p* coupling between Cu and O moves O 2*p* up, which narrows the direct fundamental band gap and (2) the Cu 3*d* orbital creates impurity bands above the ZnO valance band. As a result, for heavily doped ZnO: Cu thin films, the optical band gap contains two parts—one produced by the direct fundamental band gap and the other originated from mixed impurity band gap.[10] The optical energy bandgaps $E_g$ of the films were derived assuming a
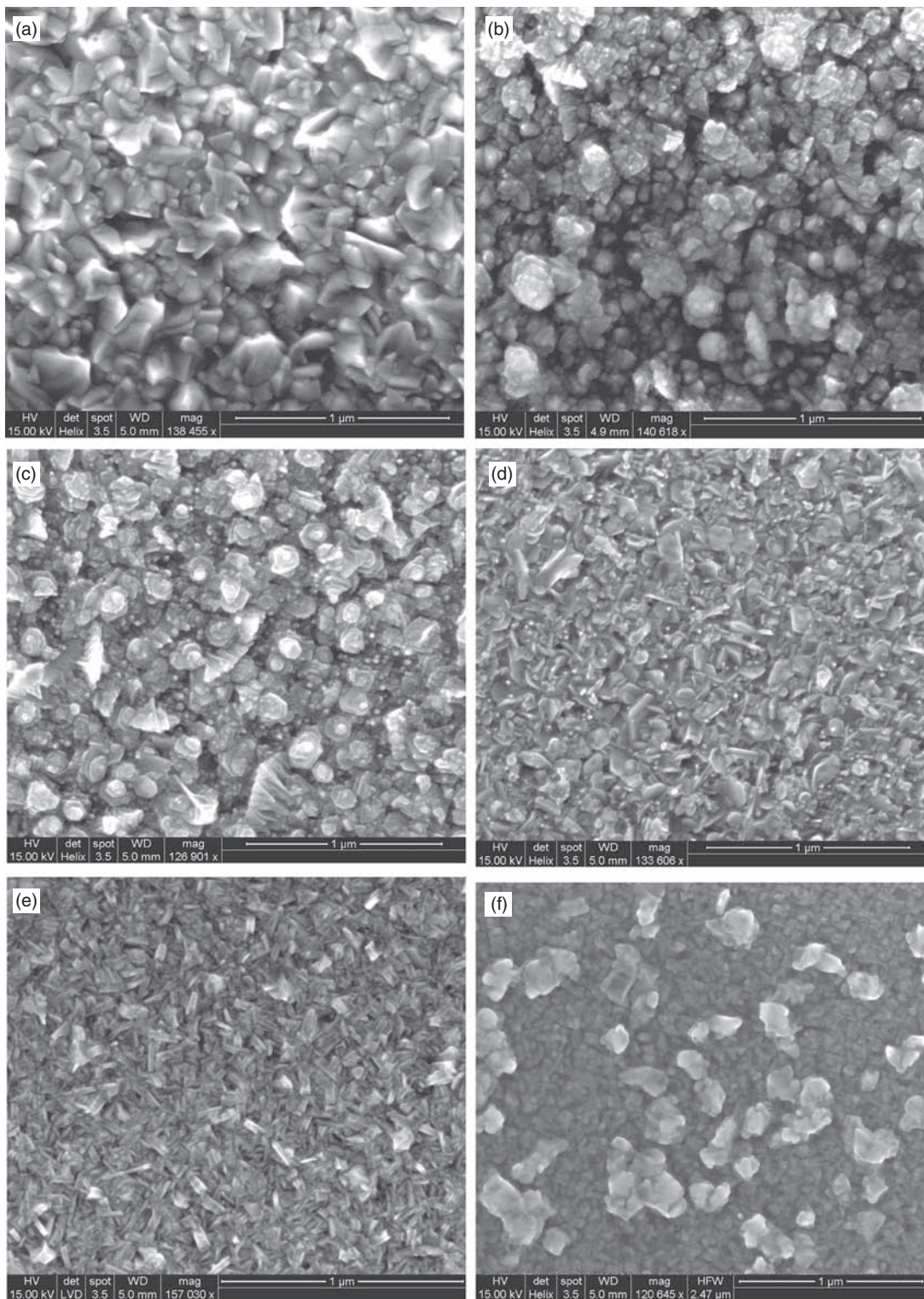
**Fig. 3.** SEM images of undoped and Cu doped ZnO films: (a) undoped ZnO, (b) ZnO: 0.5 at% Cu, (c) ZnO: 1.0 at% Cu, (d) ZnO: 2.0 at% Cu, (e) ZnO: 8.0 at% Cu and (f) ZnO: 20.0 at% Cu.

direct transition between the edges of the valence and the conduction band, using the Tauc relationship as follows:[43]

$$\alpha h\nu = A(h\nu - E_g)^n \qquad (2)$$

where $\alpha$ is the absorption coefficient, $A$ is a constant, $h$ is Planck's constant, $\nu$ is the photon frequency, and $n$ is 1/2 for direct bandgap semiconductor. An extrapolation of the linear region of a plot of $(\alpha h\nu)^{1/n}$ on the $y$-axis versus

**Table III.** XPS elemental analysis (%) of the Cu doped ZnO thin films.

| Sample | Cu/Zn expected at% | Cu/Zn measured at% | FWHM (eV) |
|---|---|---|---|
| ZnO: 2 at% Cu | 2 | 0.66 | 2.1 |
| ZnO: 4 at% Cu | 4 | 3.34 | 2.4 |
| ZnO: 8 at% Cu | 8 | 4.41 | 2.4 |
| ZnO: 16 at% Cu | 16 | 9.61 | 2.6 |
| ZnO: 20 at% Cu | 20 | 17.78 | 2.3 |



**Fig. 5.** Dynamic response of undoped ZnO sensor towards different concentrations of NO$_2$ at 135 °C.

photon energy ($h\nu$) on the $x$-axis gives the value of the bandgap energy ($E_g$). Since $E_g = h\nu$ when $(\alpha h\nu)^{1/n} = 0$, the direct bandgap of the Cu doped ZnO films was estimated from the extrapolation of the linear portion of the graphs $(\alpha h\nu)^2 = 0$ as shown in Figure 4. The value of bandgap energy was found to decrease from 3.34 eV to 3.11 eV with corresponding increase in the Cu concentration from 0 to 20 at%, respectively, as shown in inset of Figure 4.

### 3.5. Gas Sensing Results

The surface of the ZnO: Cu grains is responsible for the gas sensing properties. The chemical reactions with target gases in the metal oxide surface changes the concentration of the conduction electrons. Chemisorption changes the defect states of the metal oxide's surface. The detection of an oxidizing gas such as NO$_2$ for undoped ZnO can be associated with a reaction in which conduction electrons are consumed and the subsequent detection reaction leads to increase in the barrier height and the surface resistance. NO$_2$ is a radical molecule and its bonding interactions with the metal centres of ZnO are much stronger than those seen for other molecules such as CO, NH$_3$, H$_2$O, and H$_2$.[15, 44]

In our case, gas-sensing experiments were performed in dry air atmosphere to avoid any interference from humidity. Exposure to NO$_2$ revealed an increase in the resistivity for the undoped ZnO and a decrease for the Cu doped ZnO, indicating *n*-type conduction for undoped ZnO sample and *p*-type conduction of Cu doped samples. Figure 5 shows the dynamic response of the undoped ZnO sensor towards different concentrations of NO$_2$ at 135 °C and Figures 6(a and b) show dynamic responses of ZnO: Cu (8 and 20 at%) sensors towards different concentrations of NO$_2$ at 260 °C. The response to NO$_2$ at the tested range of temperature can be explained by the following reactions:[45]

$$NO_{2\ (gas)} + e^- \rightarrow NO_{2\ (ads)}^- \tag{3}$$

$$NO_{2\ (gas)} + O_{2\ (ads)}^- + 2e^- \rightarrow NO_{2\ (ads)}^- + 2O_{(ads)}^- \tag{4}$$

NO$_2$ molecules can interact mainly with the Zn atoms (Eq. (3)) or with oxygen species previously adsorbed. At the tested range of temperature, the main oxygen species at ZnO surface is O$_2^-$ (Eq. (4)). Note that while this electron
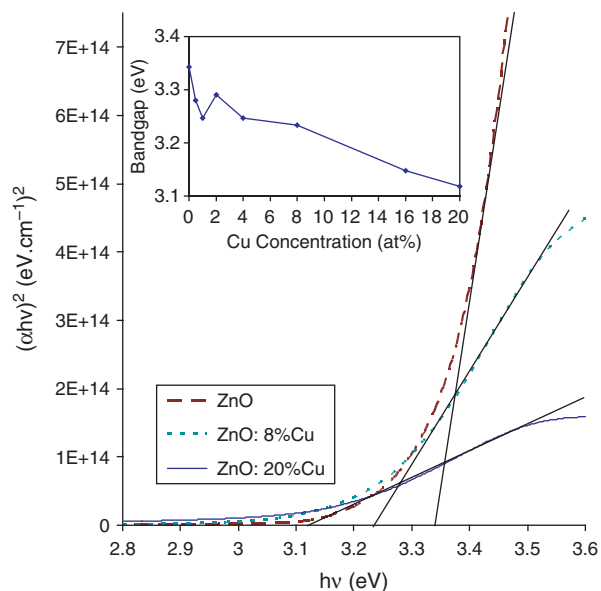


**Fig. 4.** $(\alpha h\nu)^2$ versus $h\nu$ plots of undoped and Cu doped (8 and 20 at%) ZnO thin films deposited on glass at 450 °C. The inset shows the variation of bandgap with Cu concentration.
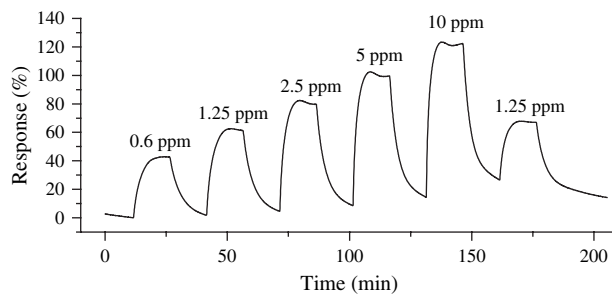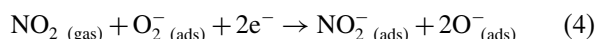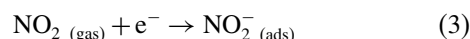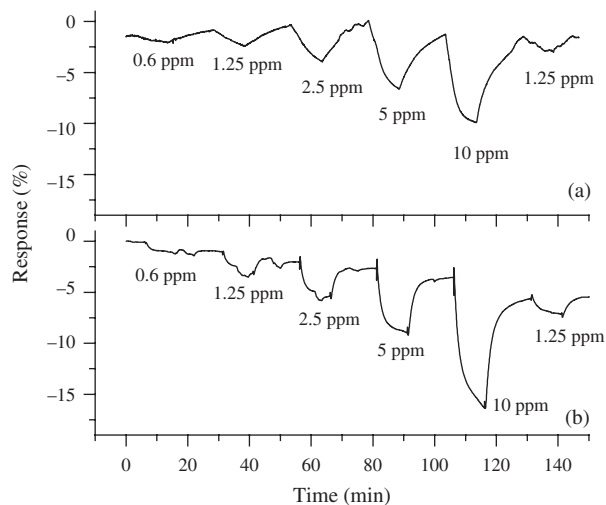


**Fig. 6.** Dynamic response of Cu doped ZnO sensors towards different concentrations of NO$_2$ at 260 °C for (a) ZnO: 8 at% Cu and (b) ZnO: 20 at% Cu.

depletion decreases the majority carrier concentration in *n*-type films (electrons) increasing the resistivity, it increases the concentration of holes (since $np = $ constant), and therefore the resistivity of the *p*-type films decreases upon exposure to NO$_2$.[13,33,45,46]

Observed changes in the sensitivity of various concentrations of Cu in ZnO may be attributed to the creation of acceptor states by Cu that are responsible for the *p*-type behaviour. The origin of the *p*-type behaviour is attributed to the holes generated by the replacement of Cu atoms by either substitutional or interstitial Zn atoms in the ZnO lattice structure. The observed decrease of resistance indicates *p*-type behaviour of the ZnO: Cu thin films. For the undoped ZnO film, the largest sensitivity was observed at 135 °C. While the largest *p*-type sensitivities were observed for the 8 and 20 at% Cu doped samples at 260 °C.

In order to increase the sensitivity, further work should be carried out regarding the enhancement of the *p*-type ZnO electrical conductivity. It is also suggested that the application of different catalysts should be investigated.

## 4. CONCLUSION

The Cu doped ZnO thin films were deposited on glass substrates using a spray pyrolysis coating system. The microstructural characterization of samples showed that the ZnO films had a polycrystalline wurtzite structure. With the increasing of the amount of Cu, crystallite size decreased, FWHM of the (002) peak became wider and the orientation poorer. The presence of Cu was also confirmed by X-ray photoelectron spectroscopy (XPS). Seebeck effect measurements confirmed the *p*-type conduction of Cu doped ZnO thin films. Gas-sensing characteristics of Cu doped (larger than 8 at%) ZnO thin films show a *p*-type response to NO$_2$. The origin of this *p*-type behaviour was attributed to the holes generated by replacement of Cu by either substitutional or interstitial Zn atoms in the ZnO thin films.

## References and Notes

1. X. H. Wang, B. Yao, Z. P. Wei, D. Z. Sheng, Z. Z. Zhang, B. H. Li, Y. M. Lu, D. X. Zhao, J. Y. Zhang, X. W. Fan, L. X. Guan, and C. X. Cong, *J. Physics D-Applied Physics* 39/21, 4568 (**2006**).
2. A. Krtschil, A. Dadgar, N. Oleynik, J. Blasing, A. Diez, and A. Krost, *Appl. Phys. Lett.* 87/26, 262105 (**2005**).
3. C. Jagadish and S. Pearton (eds.), Zinc Oxide-Bulk, Thin Films and Nanostructures, Elsevier (**2006**).
4. X. P. Peng, J. Z. Xu, H. Zang, B. Y. Wang, and Z. G. Wang, *J. Luminescence* 128/3, 297 (**2008**).
5. O. Schmidt, P. Kiesel, D. Ehrentraut, T. Fukuda, and N. M. Johnson, *Applied Physics A-Materials Science and Processing* 88/1, 71 (**2007**).
6. G. H. Kim, D. L. Kim, B. D. Ahn, S. Y. Lee, and H. J. Kim, *Microelectron. J.* 40/2, 272 (**2009**).
7. P. Fons, A. Yamada, K. Iwata, K. Matsubara, S. Niki, K. Nakahara, and H. Takasu, *Nucl. Instrum. Methods Phys. Res., Sect. B: Beam Interactions with Materials and Atoms* 199, 190 (**2003**).
8. M. Oztas and M. Bedir, *Thin Solid Films* 516/8, 1703 (**2008**).
9. J. B. Kim, D. Byun, S. Y. Ie, D. H. Park, W. K. Choi, C. Ji-Won, and A. Basavaraj, *Semicond. Sci. Technol.* 9, 095004 (**2008**).
10. K. S. Ahn, T. Deutsch, Y. Yan, C. S. Jiang, C. L. Perkins, J. Turner, and M. Al-Jassim, *J. Appl. Phys.* 102/2, 6 (**2007**).
11. H. Y. Bae and G. M. Choi, *Sens. Actuators, B: Chemical* 55/1, 47 (**1999**).
12. H. Xue, Y. Chen, X. L. Xu, G. H. Zhang, H. Zhang, and S. Y. Ma, *Physica E: Low-dimensional Systems and Nanostructures* 41/5, 788 (**2009**).
13. K. Galatsis, L. Cukrov, W. Wlodarski, P. McCormick, K. Kalantar-Zadeh, E. Comini, and G. Sbarveglieri, *Sens. Actuators, B: Chemical* 93/1–3, 562 (**2003**).
14. A. Z. Sadek, W. Wlodarski, Y. X. Li, W. Yu, X. Li, X. Yu, and K. Kalantar-Zadeh, *Thin Solid Films* 515/24, 8705 (**2007**).
15. A. Z. Sadek, S. Choopun, W. Wlodarski, S. J. Ippolito, and K. Kalantar-Zadeh, *IEEE Sens. J.* 7/5–6, 919 (**2007**).
16. S. J. Ippolito, S. Kandasamy, K. Kalantar-Zadeh, W. Wlodarski, K. Galatsis, G. Kiriakidis, N. Katsarakis, and M. Suchea, *Sens. Actuators, B: Chemical* 111–112, 207 (**2005**).
17. S. J. Ippolito, S. Kandasamy, K. Kalantar-Zadeh, and W. Wlodarski, *Sens. Actuators, B: Chemical* 108/1–2, 154 (**2005**).
18. S. J. Ippolito, S. Kandasamy, K. Kalantar-Zadeh, A. Trinchi, and W. Wlodarski, *Sensor Lett.* 1/1, 33 (**2003**).
19. J. Tan, W. Wlodarski, and K. Kalantar-Zadeh, *Thin Solid Films* 515/24, 8738 (**2007**).
20. R. Arsat, S. J. Tan, W. Modarski, and K. Kalantar-Zadeh, *Sensor Lett.* 4, 419 (**2006**).
21. J. Yu, S. J. Ippolito, M. Shafiei, D. Dhawan, W. Wlodarski, and K. Kalantar-Zadeh, *Appl. Phys. Lett.* 94/1 (**2009**).
22. Y. Shen, T. Yamazaki, Z. Liu, D. Meng, T. Kikuta, and N. Nakatani, *Thin Solid Films* 517/6, 2069 (**2009**).
23. L. A. Obvintseva, *Russian J. General Chemistry* 78/12, 2545 (**2008**).
24. H. Gong, J. Q. Hu, J. H. Wang, C. H. Ong, and F. R. Zhu, *Sens. Actuators, B: Chemical* 115/1, 247 (**2006**).
25. A. Wisitsoraat, A. Tuantranont, E. Comini, G. Sberveglieri, and W. Wlodarski, *Thin Solid Films* 517/8, 2775 (**2009**).
26. E. Comini, G. Sberveglieri, M. Ferroni, V. Guidi, and G. Martinelli, *Sens. Actuators, B: Chemical* 68/1–3, 175 (**2000**).
27. S. T. Shishiyanu, T. S. Shishiyanu, and O. I. Lupan, *Sens. Actuators, B: Chemical* 107/1, 379 (**2005**).
28. C. H. Ong, J. H. Wang, H. Gong, and H. S. O. Chang, *Int. J. Mod. Phys. B* 16/1–2, 314 (**2002**).
29. S. Singh, T. Ganguli, R. Kumar, R. S. Srinivasa, and S. S. Major, *Thin Solid Films* 517/2, 661 (**2008**).
30. R. K. Gupta, K. Ghosh, and P. K. Kahol, *Physica E: Low-dimensional Systems and Nanostructures* 41/4, 617 (**2009**).
31. M. Sahal, B. Hartiti, A. Ridah, M. Mollar, and B. Mari, *Microelectron. J.* 39/12, 1425 (**2008**).
32. J. L. Gonzalez-Vidal, M. D. Olvera, A. Maldonado, A. Reyes-Barranca, and M. Melendez-Lira, *Revista Mexicana De Fisica* 52/2, 6 (**2006**).
33. M. M. Bagheri-Mohagheghi, N. Shahtahmasebi, M. R. Alinejad, A. Youssefi, and M. Shokooh-Saremi, *Solid State Sciences* 11/1, 233 (**2009**).
34. A. Ashour, M. A. Kaid, N. Z. El-Sayed, and A. A. Ibrahim, *Appl. Surf. Sci.* 252/22, 7844 (**2006**).
35. K. Park, J. K. Seong, and S. Nahm, *J. Alloys Compd.* 455/1–2, 331 (**2008**).
36. G. Deroubaix and P. Marcus, *Surf. Interface Anal.* 18/1, 39 (**1992**).
37. J. Morales, L. Sanchez, F. Martin, J. Ramos-Barrado, and M. Sanchez, *Thin Solid Films* 474/1–2, 133 (**2005**).
38. P. P. Sahay, S. Tewari, and R. K. Nath, *Cryst. Res. Technol.* 42/7, 723 (**2007**).

**39.** Z. Banu Bahsi and A. Y. Oral, *Opt. Mater.* 29/6, 672 (**2007**).
**40.** S. C. Navale, S. W. Gosavi, and I. S. Mulla, *Talanta* 75/5, 1315 (**2008**).
**41.** G. Z. Xing, B. Yao, C. X. Cong, T. Yang, Y. P. Xie, B. H. Li, and D. Z. Shen, *J. Alloys Compd.* 457/1–2, 36 (**2008**).
**42.** G. Z. Xing, J. B. Yi, J. G. Tao, T. Liu, L. M. Wong, Z. Zhang, G. P. Li, S. J. Wang, J. Ding, T. C. Sum, C. H. A. Huan, and T. Wu, *Adv. Mater.* 20/18, 3521 (**2008**).
**43.** P. Singh, A. Kaushal, and D. Kaur, *J. Alloys Compd.* 471/1–2, 11 (**2009**).
**44.** J. A. Rodriguez, T. Jirsak, J. Dvorak, S. Sambasivan, and D. Fischer, *The Journal of Physical Chemistry B* 104/2, 319 (**2000**).
**45.** B. Ruhland, T. Becker, and G. Müller, *Sens. Actuators, B: Chemical* 50/1, 85 (**1998**).
**46.** V. Kobrinsky, A. Rothschild, V. Lumelsky, Y. Komem, and Y. Lifshitz, *Appl. Phys. Lett.* 93/11, 113502 (**2008**).

**RESEARCH ARTICLE**